

Plasma turbulence generated during particle acceleration in reconnection current sheets with magnetic islands

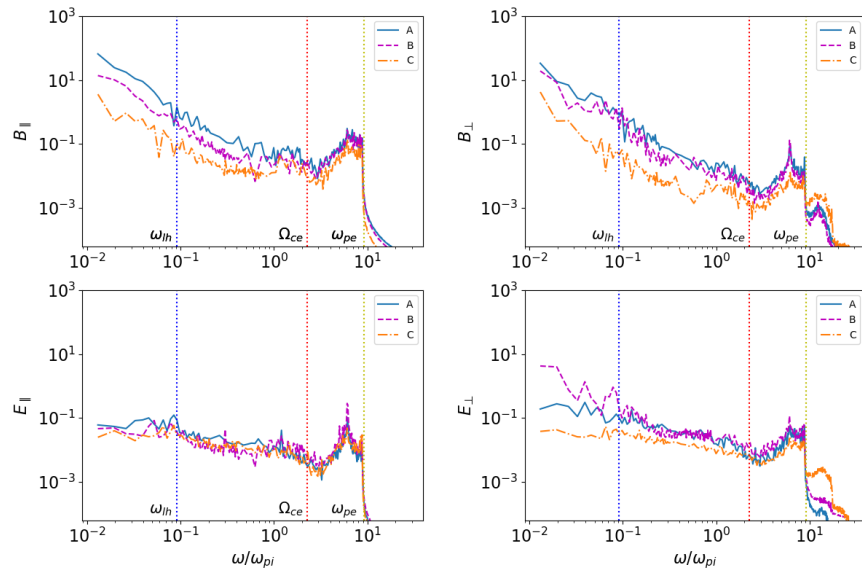
Qian Xia¹ and Valentina Zharkova¹

¹Northumbria University

November 26, 2022

Abstract

We investigate types of turbulence generated during particle acceleration in 3D Harris-type reconnecting current sheets (RCSs) with magnetic islands, using the particle-in-cell approach. When a guiding magnetic field is present in the RCS, protons and electrons become separated at ejection into the opposite semi-planes, or footpoints of reconnecting magnetic loops, due to the opposite gyration. The particles of the same charge (ions or electrons) ejected from the RCS from the opposite side where they enter called ‘transit’ particles. They are strongly energized and form unidirectional beams in the pitch-angle distribution. While the particles that move back to the same side where they enter the RCS are called ‘bounced’ particles. They gain less energy and form more diffusive pitch-angle distributions. In the RCS with magnetic islands, these two groups of particles are ejected from the X-nullpoint at the end of the islands forming the similar asymmetric distributions in the opposite separatrixes. The energy difference between ‘transit’ and ‘bounced’ particles forms ‘bump-on-tail’ velocity distributions that naturally generate plasma turbulence. Lower-hybrid waves are generated into the magnetic islands, owing to the two-stream instabilities. The presence of the anisotropic temperature inside the RCS can introduce whistler waves. High-frequency fluctuations, upper hybrid waves or electron Bernstein waves, pile up near X-nullpoints, which are consistent with MMS observations. We present the wavelet analysis and energy spectra of the turbulent electric and magnetic field fluctuations for different frequencies. The results can be beneficial for understanding in-situ observations of energetic particles in the heliosphere with modern space missions.



1
2
3
4
5
6

Plasma turbulence generated during particle acceleration in reconnection current sheets with magnetic islands

Q. Xia¹, V. Zharkova¹

¹Department of Mathematics, Physics and Electrical Engineering, Northumbria University, NE1 8ST
Newcastle upon, UK

Corresponding author: Q. Xia, q.xia@northumbria.ac.uk; xiaq0207@gmail.com

Abstract

We investigate types of turbulence generated during particle acceleration in 3D Harris-type reconnecting current sheets (RCSs) with magnetic islands, using the particle-in-cell approach. When a guiding magnetic field is present in the RCS, protons and electrons become separated at ejection into the opposite semi-planes, or footpoints of reconnecting magnetic loops, due to the opposite gyration. The particles of the same charge (ions or electrons) ejected from the RCS from the opposite side where they enter called ‘transit’ particles. They are strongly energized and form unidirectional beams in the pitch-angle distribution. While the particles that move back to the same side where they enter the RCS are called ‘bounced’ particles. They gain less energy and form more diffusive pitch-angle distributions. In the RCS with magnetic islands, these two groups of particles are ejected from the X-nullpoint at the end of the islands forming the similar asymmetric distributions in the opposite separatrices. The energy difference between ‘transit’ and ‘bounced’ particles forms ‘bump-on-tail’ velocity distributions that naturally generate plasma turbulence. Lower-hybrid waves are generated into the magnetic islands, owing to the two-stream instabilities. The presence of the anisotropic temperature inside the RCS can introduce whistler waves. High-frequency fluctuations, upper hybrid waves or electron Bernstein waves, pile up near X-nullpoints, which are consistent with MMS observations. We present the wavelet analysis and energy spectra of the turbulent electric and magnetic field fluctuations for different frequencies. The results can be beneficial for understanding in-situ observations of energetic particles in the heliosphere with modern space missions.

1 Introduction

Magnetic reconnection is a fundamental phenomenon in plasma, during which magnetic field lines change their connectivity releasing magnetic energy in the form of wave, jets and energetic particles (Priest & Forbes, 2000; Somov, 2000). The processes of magnetic reconnection are often observed during eruptive events in the Sun (flares and coronal mass ejections (CMEs)) (Antiochos et al., 1994; Antiochos, 1998; V. V. Zharkova et al., 2011; Vilmer et al., 2011; Benz, 2017), heliospheric current sheet (V. V. Zharkova & Khabarova, 2012; Zank et al., 2014; Khabarova et al., 2015, 2017), and Earth magnetosphere (Øieroset et al., 2002; Angelopoulos et al., 2008; Chen et al., 2008). Owing to large magnetic field gradients and curvatures surrounding the reconnection sites, combined with strong gradients of the plasma temperature and density, there are large variations of the electric and magnetic fields developing inside reconnecting current sheets (RCSs) during the magnetic reconnection process (Shay et al., 2016; Xia & Zharkova, 2020).

The energetic particles generated by these processes can be detected via hard X-ray (Holman et al., 2011; V. V. Zharkova et al., 2011) and γ -ray (Vilmer et al., 2011) emission in solar flares, which are often obscured by various transport effects of particles or radiations. Much more beneficial can be obtained via in-situ observations of the heliospheric structures by WIND or ACE spacecraft, or the observations in magnetosphere current sheets (CSs) by the multi-spacecraft Magnetospheric Multiscale Mission (MMS) (Øieroset et al., 2001; Burch et al., 2016), which can measure particle distributions inside reconnecting current sheets while spacecraft passing through.

The theoretical and numerical studies of magnetic reconnection are typically performed using a simplified system of 2D anti-parallel reconnecting magnetic fields with an additional guiding magnetic field in the third dimension (2.5D approach). Such RCSs with a finite B_g are not rare in Earth magnetopause (Silin & Büchner, 2006) and flare CSs at the impulsive phase of CME eruptions (Fletcher et al., 2011). The thin elongated RCSs formed in a diffusion region between the reversed magnetic field lines are shown to often break down by tearing instability into multiple islands, or O-type nullpoints, sep-

58 arated by X-nullpoints (Furth et al., 1963; Bhattacharjee et al., 2009). The presence of
 59 magnetic islands in reconnecting current sheets was demonstrated by magnetohydrody-
 60 namic (Loureiro et al., 2005; Drake et al., 2006; Lapenta, 2008; Bárta et al., 2011) and
 61 kinetic simulations (Y.-M. Huang & Bhattacharjee, 2010; Karimabadi et al., 2011; Markidis
 62 et al., 2012). Such the periodic magnetic islands were often identified in many solar flares
 63 (J. Lin et al., 2005; Oka et al., 2010; Bárta et al., 2011; Takasao et al., 2012; Nishizuka
 64 et al., 2015) and coronal mass ejections (CMEs) (Song et al., 2012). Also, they are con-
 65 firmed by the in-situ observations of CSs in the heliosphere (V. V. Zharkova & Khabarova,
 66 2012; Khabarova et al., 2015) and Earth magnetotail (Zong et al., 2004; Chen et al., 2008;
 67 R. Wang et al., 2016).

68 In the case of full 3D RCSs, the guiding field is accepted varying in time and space.
 69 In some configurations of 3D RCSs, the out-of-plane variations of the helical magnetic
 70 structures become pretty significant, due to the kink instability, obscuring current sheet
 71 structures and making hard to define clear X-nullpoints (Daughton et al., 2011a; Egedal
 72 et al., 2012). A strong guiding field B_g can suppress the out-of-plane kink instability while
 73 leaving the concept of magnetic islands still applicable (Lapenta & Brackbill, 1997; Daughton,
 74 1999; Cerutti et al., 2014; Sironi & Spitkovsky, 2014). Nevertheless, further studies have
 75 shown that both cases do not significantly change the scenarios of energy conversion and
 76 particle acceleration in 3D RCSs, because the dominant mechanisms of particle energiza-
 77 tion remain the same as in the 2.5D scenario (Hesse et al., 2001; V. V. Zharkova et al.,
 78 2011; Guo et al., 2014; Dahlin et al., 2017).

79 Depending on magnetic field topologies, the presence of a guiding field in an RCS
 80 was revealed to cause partial or full charge separation between electrons and ions (V. V. Zharkova
 81 & Gordovskyy, 2004; Pritchett & Coroniti, 2004) due to the opposite directions of gy-
 82 ration based on their opposite charges. This, in turn, can lead to the preferential ejection
 83 of the oppositely charged particles into the opposite semiplanes of CSs, or opposite
 84 footpoints of reconnecting loops. It makes the hard X-ray sources to be spatially sep-
 85 arated from the γ -ray sources in the opposite footpoints of reconnecting magnetic loops
 86 (R. P. Lin et al., 2003; Hurford et al., 2003, 2006). This charge-separation phenomenon
 87 is also confirmed in the laboratory experiments (Zhong et al., 2016). Furthermore, the
 88 separation of particles of the opposite charges introduces the polarisation electric field
 89 across the reconnection midplane, which is much larger (by two orders of magnitude) than
 90 reconnecting electric field itself (Zenitani & Hoshino, 2008; Siversky & Zharkova, 2009;
 91 Cerutti et al., 2013). The presence of polarisation electric field in RCSs has been con-
 92 firmed by in-situ observations of the ion velocity profiles during the spacecraft crossings
 93 of the heliospheric CSs, which always follow the profile of polarisation electric field (V. V. Zharkova
 94 & Khabarova, 2012; V. Zharkova & Khabarova, 2015).

95 The neutral ambient plasmas are dragged into CSs by the magnetic diffusion pro-
 96 cess from both sides of reconnecting current sheet. Although, entering the RCS from
 97 the opposite boundaries of a CS would also lead to different energy gains by the parti-
 98 cles with the same charge (Siversky & Zharkova, 2009; V. V. Zharkova & Khabarova,
 99 2012). The particles that enter an RCS from the side opposite to the that, from which
 100 they to be ejected, are classified as “transit” particles, while the particles entering the
 101 RCS from the same side where they to be ejected, are classified as “bounced” particles.

102 The transit particles gain significantly more energy because they become acceler-
 103 ated on their way to the midplane where the main acceleration occur, while bounced par-
 104 ticles lose their energy while they approach the midplane and become gaining energy from
 105 reconnection electric field (V. V. Zharkova & Gordovskyy, 2005; Siversky & Zharkova,
 106 2009; V. V. Zharkova & Khabarova, 2012). The energy difference between the transit
 107 and bounced particles creates particle beams with ‘bump-on-tail’ energy distributions,
 108 which could trigger the Buneman instability (Buneman, 1958) and generate plasma tur-
 109 bulence. In turn, this plasma turbulence can potentially contribute to further particle

110 acceleration or modify the parameters of accelerated particles (V. V. Zharkova & Agapi-
111 tov, 2009; Drake et al., 2010; Muñoz & Büchner, 2016; C. Huang et al., 2017).

112 The target of this research is to study plasma instabilities in RCSs due to the pres-
113 ence of energetic particle beams extending from the X-nullpoint into magnetic islands.
114 Because the plasma turbulence introduced by instabilities, in general, is inherently a 3D
115 problem in realistic systems (Goldreich & Sridhar, 1995), it requires the simulation do-
116 main to be 3D. As mentioned before, the out of reconnection plane variations in 3D could
117 obscure the CS structures, such as a clear X-nullpoint. Hence we implemented a strong
118 B_g to the RCSs to suppress the development of the kink mode and to stabilize the mag-
119 netic island structures along the out-of-plane direction (Xia & Zharkova, 2020). Further-
120 more, anisotropic electric and magnetic fluctuations are expected in the presence of a
121 local mean magnetic field \mathbf{B}' (Howes et al., 2008; Boldyrev et al., 2013). Thus we will
122 explore the variances developed both along and perpendicular to the mean magnetic field.
123 Besides, particles have non-Maxwellian distributions in the phase space due to the de-
124 veloped instabilities. Ng et al. (2011) has shown that a triangular-shaped distribution
125 could found close to the diffusion region in the electron velocity space, in which the fil-
126 amentary structures correspond to different groups of particles oscillating across the RCS
127 midplane. However, such structures would disappear outside of the diffusion region in
128 the presence of a weak B_g (Ng et al., 2012; S. Wang et al., 2016). Thus, the implemen-
129 tation of a strong B_g could also help the energetic particle beams to maintain the pres-
130 sure anisotropy (Le et al., 2013).

131 Similar to our previous study of electron pitch-angle distributions (PADs) in the
132 RCSs (Khabarova et al., 2020; Xia & Zharkova, 2020), we intend to consider the data
133 collected by a hypothetical spacecraft crossing the simulation domain, which allow us
134 to analyze the electric and magnetic field fluctuations with respect to the local mean mag-
135 netic field \mathbf{B}' . Because the streaming instabilities can be generated in the separatrices
136 and later extend to the exhaust region (Cattell et al., 2005; Lapenta et al., 2011; Markidis
137 et al., 2012; Zhang et al., 2019), the positions of the virtual spacecraft are set to be in
138 the exhaust close to the separatrices at different distances away from the X-nullpoints
139 that form magnetic island. So we can obtain the evolution of plasma turbulence from
140 the X-nullpoint to the O-nullpoint.

141 This paper is organized as follows. The magnetic field topology and the simulation
142 model are described in section 2. The results of simulations are analyzed in section 3.
143 A general discussion and conclusions are drawn in section 4.

144 2 Simulation model

145 To investigate turbulence generated inside RCSs with magnetic islands, let us re-
146 produce a 3D RCS model and explore the dynamics of particles accelerated during their
147 passage through this magnetic field topology. We used the models described in our pre-
148 vious papers including (Xia & Zharkova, 2020), which studied particle acceleration in
149 coalescent and squashed magnetic islands. Similarly to (Siversky & Zharkova, 2009), the
150 authors introduced static background electric and magnetic fields in the PIC code (Verboncoeur
151 et al., 1995; Bowers et al., 2008). Then they followed particle acceleration and their in-
152 duced electric and magnetic fields in 3D RCSs with a single or multiple X-nullpoints (mag-
153 netic islands). This approach allowed us to separate the original magnetic field config-
154 uration of the reconnection from that induced by the plasma feedback due to the accel-
155 erated particles and to discover triggers of plasma turbulence inside these complex mag-
156 netic configurations.

157 In the current paper, we do not separate the original and induced electromagnetic
158 fields and adopt the self-consistent PIC simulation to investigate particle acceleration
159 in magnetic islands generated by magnetic reconnection. We extend the 3D simulation

160 region to a larger domain comparing to the previous 2.5D studies by Muñoz and Büchner
 161 (2016). The simulations start with a Harris-type current sheet (CS) in the $x-z$ plane:

$$\begin{aligned} \mathbf{B}_x &= -\frac{2L_x}{L_z}\delta B_0 \sin\left(2\pi\frac{z-0.5L_z}{L_z}\right) \cos\left(\pi\frac{x}{L_x}\right), \\ \mathbf{B}_y &= B_{0y}, \\ \mathbf{B}_z &= B_{0z} \tanh\left(\frac{x}{d_{cs}}\right) + \delta B_0 \cos\left(2\pi\frac{z-0.5L_z}{L_z}\right) \sin\left(\pi\frac{x}{L_x}\right), \end{aligned} \quad (1)$$

162 where d_{cs} is the half thickness of RCS. The B_{0y} is the initial guiding field, which is per-
 163 pendicular to the reconnection plane. In the presented simulation $b_g = B_{0y}/B_{0z} = 1.0$.
 164 The initial density variation across the CS is:

$$n = n_b + n_0 \operatorname{sech}^2\left(\frac{x}{d_{cs}}\right). \quad (2)$$

165 We chose a mass ratio $m_i/m_e = 100$, a temperature ratio $T_i/T_e = 5$, a background
 166 plasma density $n_b/n_0 = 0.2$, and a frequency ratio $\omega_{pe}/\Omega_{ce} = 1.5$. The RCS initially
 167 has $d_{cs} = 0.5d_i$, where d_i is the ion inertial length. The simulation box size is $L_x \times L_y \times$
 168 $L_z = 51.2d_i \times 1.6d_i \times 12.8d_i$ with grid number $2048 \times 64 \times 512$ using 100 particles per
 169 cell. Along x , the conducting boundary condition for the electromagnetic field and open
 170 boundary condition for particles are used. The periodic boundary conditions are applied
 171 to both the electromagnetic field and particles along $z-$ and $y-$ directions.

172 To trigger magnetic reconnection, let us introduce a small interruption at the be-
 173 ginning of the simulation, which is written in terms of $(\delta B_0 \dots)$ in Eq. (1), where $\delta B_0 =$
 174 $0.03B_{0z}$. It comes from an out-of-plane vector potential, $\delta \mathbf{B}_0 = \nabla \times \delta A_y$, where $\delta A_y \propto$
 175 $\cos\left(2\pi\frac{z-0.5L_z}{L_z}\right) \cos\left(\pi\frac{x}{L_x}\right)$ satisfying $\nabla \cdot \mathbf{A} = 0$. This spatial distribution helps us to
 176 set the fast reconnection to occur near the centre of the simulation box in Figure. 1(a-
 177 d), similar to that reported earlier (Daughton et al., 2011b). Multiple small magnetic
 178 islands formed, and later merged into the island across the periodic boundary as shown
 179 in the density and energy distributions of electrons in Figure. 1(c - h). The width of this
 180 crossing-boundary island increased with time. Due to the periodic boundary condition
 181 at both ends of the $z-$ axis, the simulation domain represents the RCSs with a chain of
 182 magnetic islands, rather than a single X-nullpoint geometry with open exhausts. The
 183 energy distributions of electrons at $t = 24, 32\Omega_{ci}^{-1}$ show a clear asymmetry with respect
 184 to the midplane, due to the presence of the strong guiding field.

185 The reconnection process is still weakly affected by the kink instability at a larger
 186 time, as evidenced in the isosurface of the electron energy distribution in Figure. (2a).
 187 The distributions are similar in the different $x-z$ planes along the $y-$ direction. If the
 188 guiding field is weak, the flux ropes would be strongly interrupted. For example, we ob-
 189 served the twist of the flux ropes in the simulation box after the same running time in
 190 the $B_g = 0$ case shown in Figure. (2b). Thus the locations and the sizes of magnetic
 191 islands, if there is any, in different $x-z$ planes would change, which makes it hard to
 192 make statistical analysis depending on the distance from the X-nullpoint on different $x-$
 193 z planes along the $y-$ direction. Therefore, we will stick to $b_g = 1$ case in the follow-
 194 ing discussions as we explained in the Introduction.

195 3 Simulation results

196 3.1 Wavenumber spectra of electromagnetic fields

197 During the magnetic reconnection events as shown in Figure. 1(a-h), ion-scale mag-
 198 netic islands are formed in our simulations. For example, the size of the largest magnetic
 199 island reaches $\sim 36d_i$ after $t = 32\Omega_{ci}^{-1}$ in Figure. 1(g, h). It thus allows us to study
 200 the plasma turbulence developed in the downstream $> 15d_i$ from the X-nullpoint.

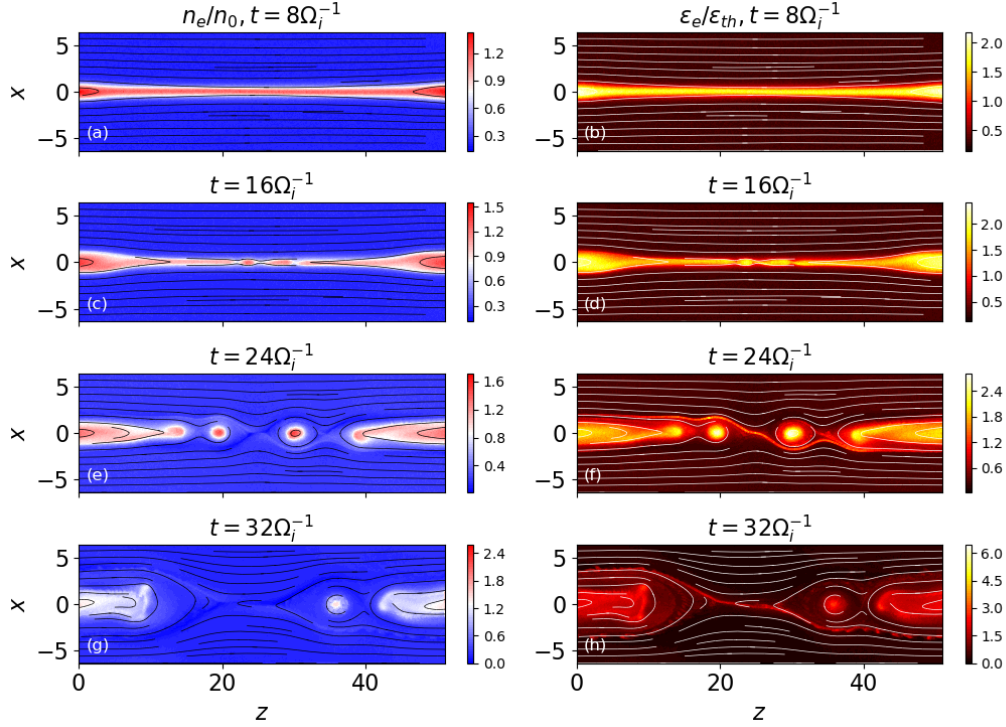


Figure 1. Density (left column) and energy (right column) distributions of electrons on the $x - z$ plane at $y = 0$ at different time: (a, b) $t = 8\Omega_{ci}^{-1}$, (c, d) $t = 16\Omega_{ci}^{-1}$, (e, f) $t = 24\Omega_{ci}^{-1}$, (g, h) $t = 32\Omega_{ci}^{-1}$ for $b_g = 1$.

201 In Figure. (3), the power spectrum of electric (magnetic) fields of the whole box
 202 are measured at $t = 32\Omega_{ci}^{-1}$ as $|\mathbf{E}|^2(k)$ ($|\mathbf{B}|^2(k)$) in the Fourier space, where k stands
 203 for the wavenumber in the reconnection plane. In this session, we did not discuss the anisotropic
 204 problem (k_{\parallel} , k_{\perp} to the local magnetic field) in this session, because there is no uniform
 205 background magnetic field across the domain as studied in homogeneous plasma turbu-
 206 lence problem, where the local magnetic field $\mathbf{B}(x, y, z) \approx \mathbf{B}' + \delta\mathbf{B}(x, y, z)$ (Goldreich
 207 & Sridhar, 1995).

208 In this model, the wave-number spectrum of the magnetic field formed a quasi-stable
 209 range from $kd_i = 1$ down to above $kd_e = 1$. A least square fitting of $|\mathbf{B}|^2(k) \propto k^{\alpha}$
 210 over this range indicates the slope $\alpha \approx -2.7$. The spectrum of the electric fields drops
 211 significantly at scales near the electron inertial scale (the solid line, $k_{de}(n_0)$, and dashed
 212 line, $k_{de}(n_b)$, on the right side of the spectra are calculated from the RCS density and
 213 background density). It suggests that during the selected time the large-scale waves are
 214 quasi-stable. Meanwhile, the spectra show that the electromagnetic energy is strongly
 215 damped at the electron characteristic scale.

216 3.2 Phase space distributions

217 As soon as particles became accelerated and were ejected from the X-nullpoint, they
 218 form the beams with different energies defined by the difference in energy gains of trans-
 219 sit and bounced particles (Xia & Zharkova, 2020) forming ‘bump-on-tail’ energy distri-
 220 butions. These beams with two-peak energy distributions can naturally trigger Buneman
 221 instabilities. In addition, highly anisotropic energy distributions in the beams, and

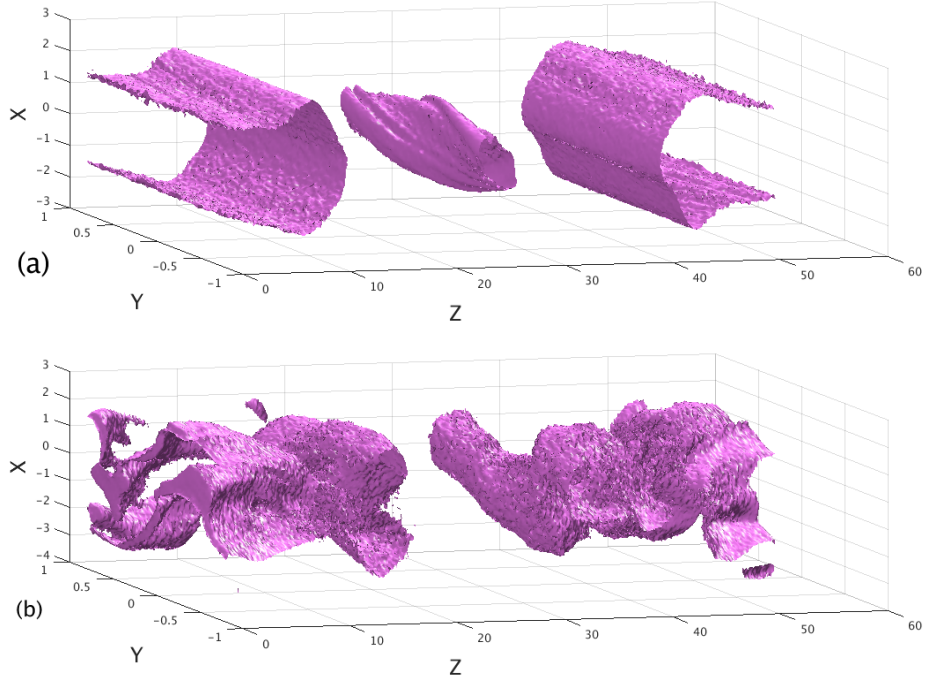


Figure 2. *Upper plot:* Isosurface of the electron energy distribution (the 35% contour of the max energy) in the simulation box of Figure. (1) at $t = 28\Omega_{ci}^{-1}$. *Bottom plot:* Isosurface of the electron energy distribution after the same running time from a similar simulation using $b_g = 0$.

222 the presence of a large density gradient between the beams and ambient plasma would
 223 introduce other instabilities, which tend to prevent beams from propagating as beams
 224 and generate plasma turbulence.

225 We examined the changes in the $v_y - x$ phase space for both ions and electrons
 226 along the cuts perpendicular to the reconnection midplane at different distances away
 227 from the X-nullpoint as shown in Figure 4. The non-Maxwellian feature first showed up
 228 in Figure 4(c): at $z = 15$ (or $\Delta z \sim 7$ away from the main X-nullpoint), electron holes
 229 are formed in the phase space near $x = -1.5$ to 1.0 , which is triggered by the beam-
 230 driven lower hybrid instability.

231 Then as the inspecting plane moves deeper into the magnetic island, the pertur-
 232 bation in the ion phase space was found at $z = 10$ (or $\Delta z \sim 12$ away from the X-nullpoint)
 233 in Figure 4(b), where the arcs in the $x = 0$ to 2 region represent different groups of ion
 234 beams. We did not find any clear ion holes in the phase space, but those arcs disappear
 235 quickly further in the downstream, which suggest the ion beams are also suppressed by
 236 plasma turbulence.

237 3.3 Frequency analysis

238 3.3.1 Wavelet analysis

239 The plasma turbulence introduced by beam instabilities can also be studied using
 240 electric and magnetic fluctuations in the frequency domain. After we identified the in-
 241 stability signals in the particle phase space, we took the advantage of wavelet analysis,

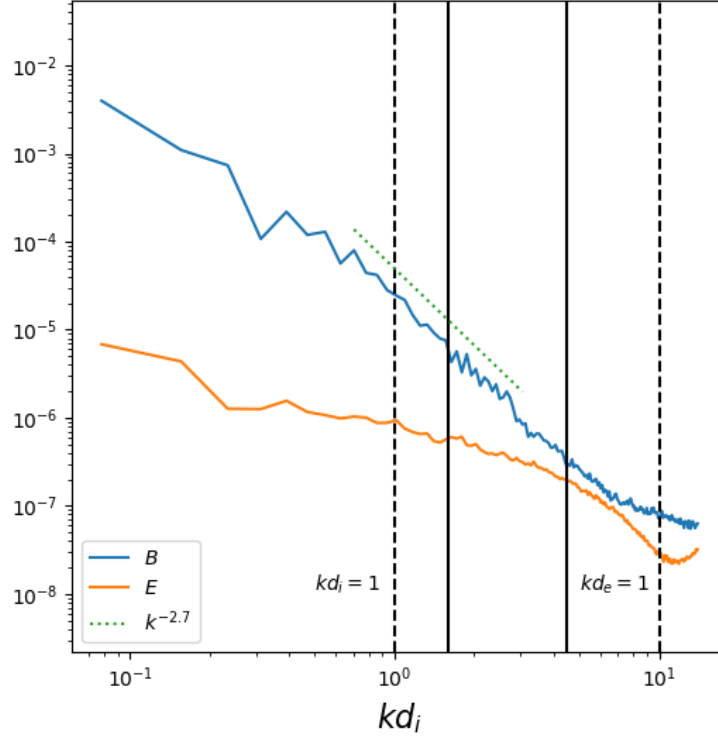


Figure 3. Power spectra of the electric (normalized by $B_0^2 V_A^2$) and magnetic fields (normalized by B_0^2). The wave vector is normalized to d_i^{-1} of n_0 . The corresponding $k_{d_i}(n_0)$, $k_{d_e}(n_0)$ are marked in dash lines. The solid lines indicate the ion gyroscale $k_{\rho_i}^{-1}$ (left) and electron inertial scale calculated by the background density $k_{d_e}(n_b)^{-1}$ (right).

242 which is a powerful tool to analyse time-series data collected by a pinpoint in the do-
 243 main, to study the fluctuations using discrete wavelet transform (Farge, 1992).

244 We explored the fluctuations of electric and magnetic fields in the exhaust obtained
 245 during the acceleration of particles in the RCS. The signals at different grids along the
 246 y -direction were transformed to wavelet power spectra using Morlet wavelet. Then the
 247 results were averaged along the out-of-plane y -axis. The wavelet power spectra of both
 248 electric and magnetic field components shared the same features. For example, Figure.
 249 (5) shows the results using the data of the B_x component recorded at point B ($z = 15, x =$
 250 0.25), where the electron holes were observed in the phase space in Figure. 4(c) for a per-
 251 iod of $5\Omega_{ci}^{-1}$.

252 Comparing to the wavenumber spectra of electromagnetic fields from the whole re-
 253 gion (section 3.1), the wavelet analysis showed that the dominant fluctuations have long
 254 periods (or low-frequency, $\ll \Omega_{ce}$). Furthermore, the wavelet transform revealed richer
 255 features in the high-frequency region. Figure. (4) depicts several high-frequency signals
 256 represented by dark purple stripes, which reached electron characteristic frequency. Thus,
 257 the electromagnetic fields spectra in wavenumber and via wavelet transform both indi-
 258 cate the important role of electrons in plasma turbulence developed in magnetic islands.

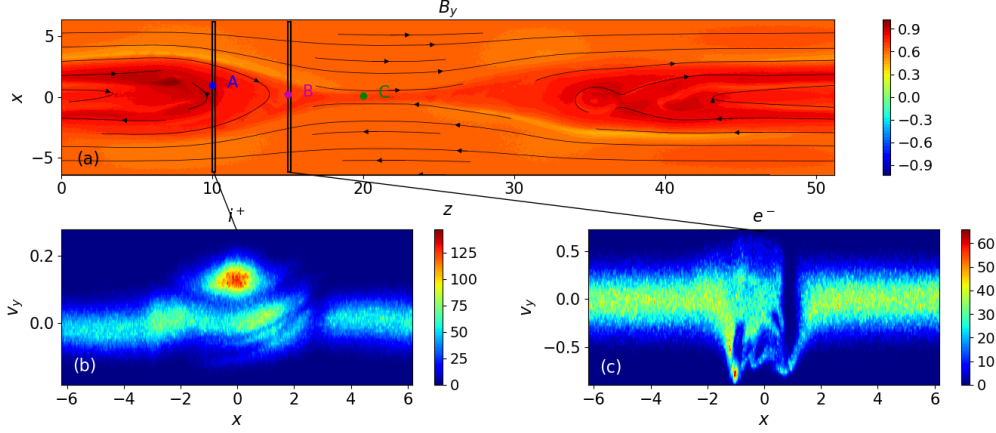


Figure 4. Phase-space distribution functions of the (b) ions and (c) electrons at different locations at $t = 36\Omega_i^{-1}$. The out-of-plane magnetic field component B_y at $y = 0$ is coloured in panel (a) with the in-plane magnetic field topology (black solid lines). The electromagnetic fields at A, B, and C are recorded for further analysis. The phase space structures in (b) and (c) are captured in the vertically elongated boxes with a width of $\Delta y = 0.2d_i$. The main X-nullpoint is located at $z = 22, x = 0$. This simulation started with a strong guiding field ($b_g = 1$).

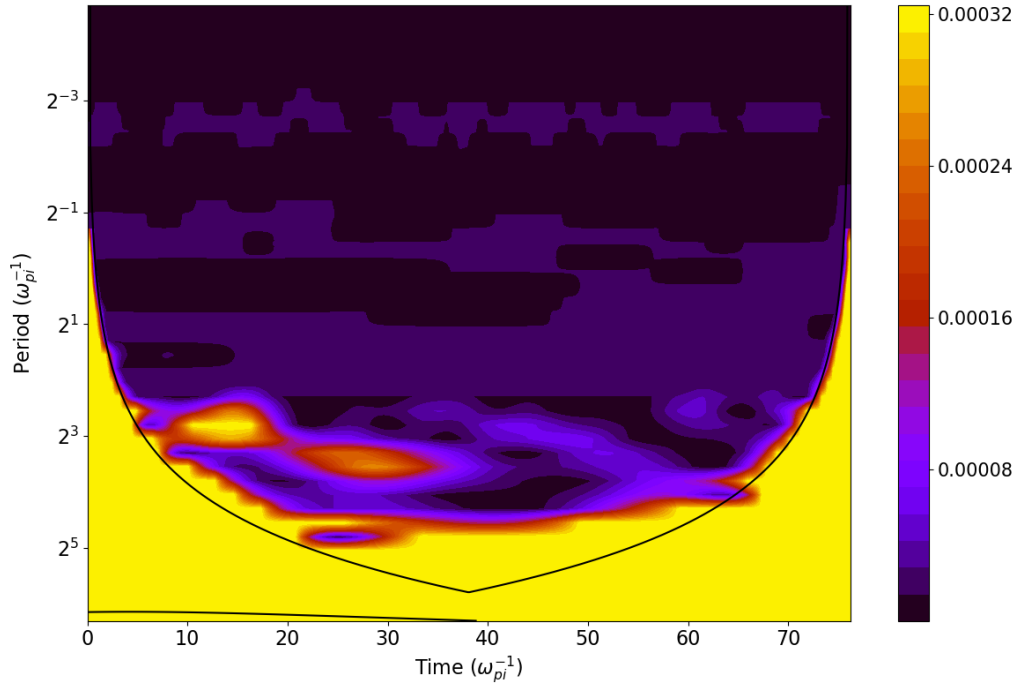


Figure 5. Local wavelet power spectrum of B_x (the purple point B at $z = 15, x = 0.25$ in Figure. 4) of the time series of B_x components, using Morlet wavelet. The solid dark curve encloses the regions of $> 95\%$ confidence.

259

3.3.2 Frequency spectra of electromagnetic fields

260

Furthermore, let us split now the electric and magnetic fields to the parallel and perpendicular components based on the local mean magnetic field \mathbf{B}' . This idea comes

261

from plasma turbulence concepts that fluctuations exhibit anisotropic features in the presence of a strong background field (sometimes also called the guide field, but it is different from the concept of the guiding field B_g in magnetic reconnection). In this section, this local mean magnetic field was averaged over both the space and the time: the surveyed box size was $\Delta L_x (= 0.2d_i) \times L_y \times \Delta L_z (= 0.2d_i)$ surrounding the selected points in Figure. (4); the values were also averaged over $5\Omega_{ci}^{-1}$ period of simulation time. Then the \mathbf{B} and \mathbf{E} components on every grid are projected to this \mathbf{B}' to get the parallel and perpendicular components. The the results in Figure. (6) were averaged over the Fourier spectra of the electric and magnetic field components from the surveyed grid points.

In this session, we assumed virtual spacecraft staying at three different locations: A, B, and C as shown in Figure. 4. From point C \rightarrow A, the selected points are further away from the X-nullpoint. The most obvious changes are in the low-frequency part: right below Ω_{ce} , we could find large enhancement in the amplitude of B_{\perp} (and a spike in E_{\parallel}), which could contribute to the generation of whistler waves in the region near points A and B. Further down in the lower frequency region, the amplitudes of B_{\parallel} , B_{\perp} , and E_{\perp} are much larger over a large range. The small bump near ω_{lh} (especially in the electric fields near point A at $z = 10, x = 1$) represent the lower hybrid waves.

In the very-high-frequency part ($\geq \omega_{pe}$), we first noticed that the perpendicular electric field E_{\perp} at $f > \omega_{pe}$ is damped significantly as it moves away from the X-nullpoint. In other words, these waves represented by E_{\perp} are only observable near X-nullpoints. Furthermore, both high-frequency fluctuations of $\delta\mathbf{E}$ and $\delta\mathbf{B}$ are mainly perpendicular to \mathbf{B}' . Further analysis of the fluctuations on the perpendicular plane showed that E_{\perp}, B_{\perp} are right-hand polarized, which are consistent with electron circular direction in the plane. In the sub-high-frequency region, $\Omega_{ce} < f < \omega_{pe}$, we found several distinct spikes in all the fields at three locations. Considering that the periodic boundary condition along z -axis stands for simulating a chain of magnetic islands, it suggests that the magnetic island pool is fulfilled with these electromagnetic fluctuations above Ω_{ce} . Besides, we also noticed that the enhancement near $f \approx \omega_{lh}$, $f < \Omega_{ce}$, and $\Omega_{ce} < f < \omega_{pe}$ are consistent with the dark horizontal stripes in the wavelet power spectrum in Figure. (5). By splitting the electromagnetic fluctuations into the parallel and perpendicular direction, here we further identified the differences between those stripe signals appeared in the wavelet analysis.

4 Discussion and Conclusions

In this paper, we simulated 3D RCSs with magnetic islands generated from a Harris-type CS equilibrium. Our goal was to track the plasma turbulence development following the ejection of energetic particles in magnetic islands, from the X-nullpoint to the O-nullpoint. This can provide more signatures for us to identify RCS structures, which is a challenging problem in space plasma due to the limited opportunities of spontaneous multiple spacecraft observation within a single RCS. In our previous study, we have studied the pitch-angle distributions of electrons and found characteristic signals, such as counter-streaming strahls and heat flux dropouts, which depends on the specific magnetic field topology (Khabarova et al., 2020; Xia & Zharkova, 2020). Here we shift our attention to the electric and magnetic field fluctuations in the frequency domain, with growing interests and available data in the community.

Particles that drift into the RCSs from opposite boundaries would gain different energy gains in the presence of a magnetic guiding field Siversky and Zharkova (2009). Previous 2.5D PIC simulation by Siversky and Zharkova (2009) of particle acceleration near a single X-nullpoint have shown these accelerated particle beams with different energies form a bump-on-tail distribution at the ejection, which leads to Buneman instabilities (Buneman, 1958) and generates turbulence (Jaroschek et al., 2004; Siversky & Zharkova, 2009; Drake et al., 2010). Later Muñoz and Büchner (2016) showed that non-

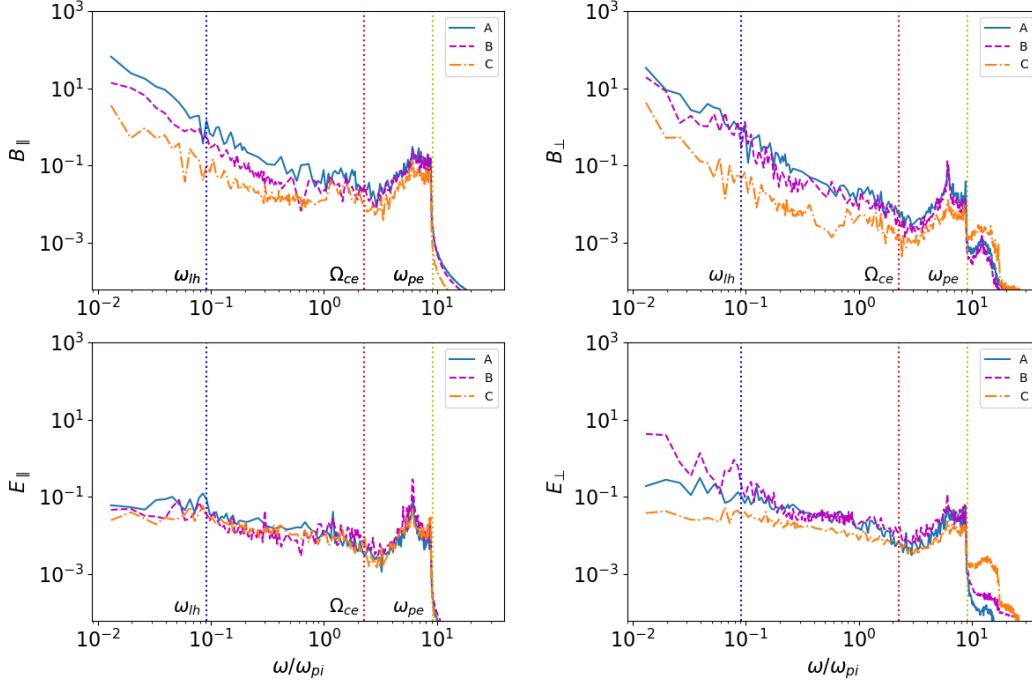


Figure 6. The spectra of different \mathbf{E} and \mathbf{B} components at selected points (marked in corresponding colors in Figure. 4) as functions of the frequency (normalized to ω_{pi}): B_{\parallel} , E_{\parallel} , B_{\perp} , E_{\perp} with respect to the local mean magnetic field in 3D. The characteristic lower-hybrid frequency ω_{lh} , electron gyro frequency Ω_{ce} , and electron plasma frequency ω_{pe} are labelled as vertical dotted lines.

313 Maxwellian distributions appeared in the electron phase space at a distance $\sim 6d_i$ away
 314 from the X-nullpoint, generating lower hybrid waves. Therefore, we set a larger 3D sim-
 315 ulation domain, in which magnetic reconnection generated a large magnetic island with
 316 size $\sim 32d_i$. A strong guiding field B_g is implemented to suppress the kink instability
 317 and keep the geometry quasi-similar on each $x - z$ plane. It allows us to get statisti-
 318 cal results by averaging the data collected from 64 grid points along the y -direction.

319 In this large 3D simulation box, the turbulent magnetic field in the RCS formed
 320 a steady spectral slope $\propto k^{-2.7}$ near the ion inertial length, and a steeper cascade at
 321 electron scales at $t = 36\Omega_{ci}^{-1}$, which is consistent with the other 3D PIC simulations (Karimabadi
 322 et al., 2013; X. Li et al., 2019), suggesting quasi-stable turbulence is built up at this mo-
 323 ment. Hence we inspected the phase space of particles at this selected time, and iden-
 324 tified two regions with clear non-Maxwellian distributions: the electron beams evolved
 325 into phase-space holes $\sim 7d_i$ away from the main X-nullpoint, which indicates that stream-
 326 ing instabilities broke the beam structures. This was consistent with the previous num-
 327 erical findings (Drake et al., 2003; Muñoz & Büchner, 2016) and observations in the
 328 Earth’s magnetotail (Khotyaintsev et al., 2010). Furthermore, we also that found the
 329 arc-shape distributions, which represent different ion beams, showed up in the phase space
 330 at $12d_i$ from the X-nullpoint and disappeared shortly in the further downstream. Thus
 331 the ion beams would also be quickly suppressed by two-stream instabilities. The differ-
 332 ence between the electron and ion phase space suggests that to understand the full pic-
 333 ture of plasma turbulence due to magnetic reconnection, it requires the simulation size
 334 to be much bigger than the diffusion region (Eastwood et al., 2018; Zhang et al., 2019).

335 By analysis the changes of the electric and magnetic fields at different locations,
 336 we could connect these non-Maxwellian features with distinct fluctuations. The electric
 337 and magnetic field information collected by a virtual spacecraft between the X-nullpoint
 338 and the O-nullpoint were transformed to the frequency domain. The wavelet power spec-
 339 trum in the exhaust showed that low-frequency fluctuations dominate the region. Sev-
 340 eral distinct groups of fluctuations with higher frequencies could be identified within the
 341 surveyed period. Because of the anisotropy of plasma turbulence in the presence of a strong
 342 magnetic field (Boldyrev et al., 2013; Loureiro, Nuno F. & Boldyrev, Stanislav, 2017),
 343 we compared the parallel and perpendicular components of the electric and magnetic field
 344 data separately. These data are collected by three virtual spacecraft, which are positioned
 345 from near X-nullpoint to deep in the exhaust region.

346 The electron beams are found to introduce high-frequency electromagnetic fluctu-
 347 ations above Ω_{ce} , which are observed through all of the three surveyed points in Figure.
 348 (3). These fluctuations spread from the electron gyro frequency to upper hybrid frequency.
 349 Similar signals are found in the inflow region close to the X-nullpoint rather than the
 350 exhaust by Lapenta et al. (2020). It suggests that these high-frequency harmonic sig-
 351 nals could result from the periodic boundary condition, which represents a region filled
 352 with magnetic island structures in the RCS. It thus prevents the waves from escaping
 353 to the open field regions.

354 Such high-frequency harmonics above Ω_{ce} have recently been discovered by MMS
 355 satellites near the electron diffusion region in the magnetopause (Dokgo et al., 2019). The
 356 authors identified these high-frequency fluctuations as the harmonics of upper hybrid waves,
 357 although they exhibited electromagnetic features. On the other hand, W. Y. Li et al. (2020)
 358 reported the signals in E_{\perp} and B_{\perp} power spectra peak at the harmonics of $n\Omega_{ce}$, where
 359 $n = 1, 2, 3, \dots$ near an electron diffusion region in the magnetotail. Thus they are con-
 360 tributed to electron Bernstein waves. One difference in the observation is that $\omega_{pe}/\Omega_{ce} \approx$
 361 27 in the magnetosphere, which keeps those two signals well separated. But this ratio
 362 is much low in most PIC simulations (here it is 3.5) so we could not distinguish them-
 363 clearly.

364 The frequency spectra of electric and magnetic fields obtained at different locations
 365 also revealed that turbulence was changing in the outflow from the X-nullpoint to O-nullpoint.
 366 The ultra-high frequency electrostatic fluctuations in the E_{\perp} component, e.g. the high
 367 harmonics of electron Bernstein waves (Bernstein, 1958; Guskov & Surkov, 2007), were
 368 found to only exist near the X-nullpoint. This is consistent with the MMS observations
 369 mentioned above. As the observer moved away from the X-nullpoint, the whistler waves
 370 were developing into peaks near the sub- Ω_{ce} (Fujimoto & Sydora, 2008; Muñoz & Büchner,
 371 2016; Graham et al., 2016). These waves could be generated by the temperature anisotropic
 372 instabilities (Gary & Karimabadi, 2006) and are also consistent with the electron holes
 373 in the phase space (Goldman et al., 2014). Meanwhile, low-frequency waves dominated
 374 the regions further in the outflow. The amplitudes of the fluctuations increased near the
 375 lower-hybrid frequency (Rogers et al., 2000). The lower-hybrid waves could be generated
 376 by two-stream instabilities as shown in the energy distribution of Figure. (2b) (Papadopoulos
 377 & Palmadesso, 1976; Zhou et al., 2014; Xia & Zharkova, 2020), or due to the strong den-
 378 sity gradient near the separatrices and in the outflow (Scholer et al., 2003; Divin et al.,
 379 2015).

380 In summary, we have identified the plasma turbulence in the RCS with magnetic
 381 islands and linked the characteristic fluctuations to the non-Maxwellian distributions of
 382 particles in phase space. The observed waves vary as a function of the distance away from
 383 the X-nullpoint. The high-frequency perpendicular fluctuations damp quickly out of the
 384 electron diffusion region, and the lower-frequency whistler and lower-hybrid waves are
 385 developing because of the streaming instabilities and strong plasma temperature anisotropy
 386 and density gradient. These signals offer new observational evidence of the existing of
 387 local particle acceleration due to magnetic reconnection in the solar wind. These works

388 potentially benefit the in-situ study of RCSs near the Sun from Parker Solar Probe (Phan
389 et al., 2020).

390 Acknowledgments

391 The authors acknowledge the funding for this research provided by the U.S. Air Force
392 grant *PRJ02156*. This work used the DiRAC Complexity system, operated by the Uni-
393 versity of Leicester IT Services, which forms part of the STFC DiRAC HPC Facility (*www.dirac.ac.uk*).
394 This equipment is funded by BIS National E-Infrastructure capital grant ST/K000373/1
395 and STFC DiRAC Operations grant ST/K0003259/1. DiRAC is part of the National
396 e-Infrastructure.

397 References

- 398 Angelopoulos, V., McFadden, J. P., Larson, D., Carlson, C. W., Mende, S. B., Frey,
399 H., ... Kepko, L. (2008, August). Tail Reconnection Triggering Substorm
400 Onset. *Science*, *321*, 931. doi: 10.1126/science.1160495
- 401 Antiochos, S. K. (1998, August). The Magnetic Topology of Solar Eruptions. *Astro-*
402 *physical Journal, Letters*, *502*, L181-L184. doi: 10.1086/311507
- 403 Antiochos, S. K., Dahlburg, R. B., & Klimchuk, J. A. (1994, January). The mag-
404 netic field of solar prominences. *Astrophysical Journal, Letters*, *420*, L41-L44.
405 doi: 10.1086/187158
- 406 Bárta, M., Büchner, J., Karlický, M., & Skála, J. (2011, August). Sponta-
407 neous Current-layer Fragmentation and Cascading Reconnection in So-
408 lar Flares. I. Model and Analysis. *Astrophysical Journal*, *737*, 24. doi:
409 10.1088/0004-637X/737/1/24
- 410 Benz, A. O. (2017, December). Flare Observations. *Living Reviews in Solar Physics*,
411 *14*, 2. doi: 10.1007/s41116-016-0004-3
- 412 Bernstein, I. B. (1958, January). Waves in a Plasma in a Magnetic Field. *Physical*
413 *Review*, *109*(1), 10-21. doi: 10.1103/PhysRev.109.10
- 414 Bhattacharjee, A., Huang, Y.-M., Yang, H., & Rogers, B. (2009). Fast reconnection
415 in high-lundquist-number plasmas due to the plasmoid instability. *Physics*
416 *of Plasmas*, *16*(11), 112102. Retrieved from [https://doi.org/10.1063/](https://doi.org/10.1063/1.3264103)
417 [1.3264103](https://doi.org/10.1063/1.3264103) doi: 10.1063/1.3264103
- 418 Boldyrev, S., Horaites, K., Xia, Q., & Perez, J. C. (2013, November). Toward a
419 Theory of Astrophysical Plasma Turbulence at Subproton Scales. *Astrophysical*
420 *Journal*, *777*(1), 41. doi: 10.1088/0004-637X/777/1/41
- 421 Bowers, K. J., Albright, B. J., Yin, L., Bergen, B., & Kwan, T. J. T. (2008, May).
422 Ultrahigh performance three-dimensional electromagnetic relativistic kinetic
423 plasma simulation). *Physics of Plasmas*, *15*, 055703. doi: 10.1063/1.2840133
- 424 Buneman, O. (1958, Jul). Instability, turbulence, and conductivity in current-
425 carrying plasma. *Phys. Rev. Lett.*, *1*, 8-9. Retrieved from [https://link.aps](https://link.aps.org/doi/10.1103/PhysRevLett.1.8)
426 [.org/doi/10.1103/PhysRevLett.1.8](https://link.aps.org/doi/10.1103/PhysRevLett.1.8) doi: 10.1103/PhysRevLett.1.8
- 427 Burch, J. L., Moore, T. E., Torbert, R. B., & Giles, B. L. (2016, March). Magne-
428 topheric Multiscale Overview and Science Objectives. *Space Science Reviews*,
429 *199*(1-4), 5-21. doi: 10.1007/s11214-015-0164-9
- 430 Cattell, C., Dombeck, J., Wygant, J., Drake, J. F., Swisdak, M., Goldstein, M. L.,
431 ... Balogh, A. (2005). Cluster observations of electron holes in association
432 with magnetotail reconnection and comparison to simulations. *Journal of*
433 *Geophysical Research: Space Physics*, *110*(A1). Retrieved from [https://](https://agupubs.onlinelibrary.wiley.com/doi/abs/10.1029/2004JA010519)
434 agupubs.onlinelibrary.wiley.com/doi/abs/10.1029/2004JA010519 doi:
435 [10.1029/2004JA010519](https://doi.org/10.1029/2004JA010519)
- 436 Cerutti, B., Werner, G. R., Uzdensky, D. A., & Begelman, M. C. (2013, June).
437 Simulations of Particle Acceleration beyond the Classical Synchrotron Burnoff
438 Limit in Magnetic Reconnection: An Explanation of the Crab Flares. *Astro-*

- 439 *physical Journal*, 770(2), 147. doi: 10.1088/0004-637X/770/2/147
- 440 Cerutti, B., Werner, G. R., Uzdensky, D. A., & Begelman, M. C. (2014, Febru-
441 ary). Three-dimensional Relativistic Pair Plasma Reconnection with Radiative
442 Feedback in the Crab Nebula. *Astrophysical Journal*, 782(2), 104. doi:
443 10.1088/0004-637X/782/2/104
- 444 Chen, L.-J., Bhattacharjee, A., Puhl-Quinn, P. A., Yang, H., Bessho, N., Imada, S.,
445 ... Georgescu, E. (2008, January). Observation of energetic electrons within
446 magnetic islands. *Nature Physics*, 4, 19-23. doi: 10.1038/nphys777
- 447 Dahlin, J. T., Drake, J. F., & Swisdak, M. (2017, September). The role of
448 three-dimensional transport in driving enhanced electron acceleration dur-
449 ing magnetic reconnection. *Physics of Plasmas*, 24(9), 092110. doi:
450 10.1063/1.4986211
- 451 Daughton, W. (1999, April). The unstable eigenmodes of a neutral sheet. *Physics of*
452 *Plasmas*, 6(4), 1329-1343. doi: 10.1063/1.873374
- 453 Daughton, W., Roytershteyn, V., Karimabadi, H., Yin, L., Albright, B. J., Bergen,
454 B., & Bowers, K. J. (2011a, July). Role of electron physics in the development
455 of turbulent magnetic reconnection in collisionless plasmas. *Nature Physics*, 7,
456 539-542. doi: 10.1038/nphys1965
- 457 Daughton, W., Roytershteyn, V., Karimabadi, H., Yin, L., Albright, B. J., Bergen,
458 B., & Bowers, K. J. (2011b, July). Role of electron physics in the development
459 of turbulent magnetic reconnection in collisionless plasmas. *Nature Physics*, 7,
460 539-542. doi: 10.1038/nphys1965
- 461 Divin, A., Khotyaintsev, Y. V., Vaivads, A., André, M., Markidis, S., & Lapenta, G.
462 (2015, April). Evolution of the lower hybrid drift instability at reconnection
463 jet front. *Journal of Geophysical Research (Space Physics)*, 120(4), 2675-2690.
464 doi: 10.1002/2014JA020503
- 465 Dokgo, K., Hwang, K.-J., Burch, J. L., Choi, E., Yoon, P. H., Sibeck, D. G., & Gra-
466 ham, D. B. (2019, July). High-Frequency Wave Generation in Magnetotail
467 Reconnection: Nonlinear Harmonics of Upper Hybrid Waves. *Geophysics*
468 *Research Letters*, 46(14), 7873-7882. doi: 10.1029/2019GL083361
- 469 Drake, J. F., Opher, M., Swisdak, M., & Chamoun, J. N. (2010, February). A Mag-
470 netic Reconnection Mechanism for the Generation of Anomalous Cosmic Rays.
471 *Astrophysical Journal*, 709, 963-974. doi: 10.1088/0004-637X/709/2/963
- 472 Drake, J. F., Swisdak, M., Cattell, C., Shay, M. A., Rogers, B. N., & Zeiler,
473 A. (2003). Formation of electron holes and particle energization dur-
474 ing magnetic reconnection. *Science*, 299(5608), 873-877. Retrieved
475 from <https://science.sciencemag.org/content/299/5608/873> doi:
476 10.1126/science.1080333
- 477 Drake, J. F., Swisdak, M., Che, H., & Shay, M. A. (2006, October). Electron ac-
478 celeration from contracting magnetic islands during reconnection. *Nature*, 443,
479 553-556. doi: 10.1038/nature05116
- 480 Eastwood, J. P., Mistry, R., Phan, T. D., Schwartz, S. J., Ergun, R. E., Drake,
481 J. F., ... Russell, C. T. (2018). Guide field reconnection: Exhaust structure
482 and heating. *Geophysical Research Letters*, 45(10), 4569-4577. Retrieved
483 from [https://agupubs.onlinelibrary.wiley.com/doi/abs/10.1029/](https://agupubs.onlinelibrary.wiley.com/doi/abs/10.1029/2018GL077670)
484 [2018GL077670](https://agupubs.onlinelibrary.wiley.com/doi/abs/10.1029/2018GL077670) doi: 10.1029/2018GL077670
- 485 Egedal, J., Daughton, W., & Le, A. (2012, April). Large-scale electron accelera-
486 tion by parallel electric fields during magnetic reconnection. *Nature Physics*, 8,
487 321-324. doi: 10.1038/nphys2249
- 488 Farge, M. (1992). Wavelet transforms and their applications to turbulence. *Annual*
489 *Review of Fluid Mechanics*, 24(1), 395-458. Retrieved from [https://doi.org/](https://doi.org/10.1146/annurev.fl.24.010192.002143)
490 [10.1146/annurev.fl.24.010192.002143](https://doi.org/10.1146/annurev.fl.24.010192.002143) doi: 10.1146/annurev.fl.24.010192
491 .002143
- 492 Fletcher, L., Dennis, B. R., Hudson, H. S., Krucker, S., Phillips, K., Veronig, A., ...
493 Temmer, M. (2011, September). An Observational Overview of Solar Flares.

- 494 *Space Science Reviews*, 159(1-4), 19-106. doi: 10.1007/s11214-010-9701-8
- 495 Fujimoto, K., & Sydora, R. D. (2008, October). Whistler waves associated with
496 magnetic reconnection. *Geophysics Research Letters*, 35(19), L19112. doi: 10
497 .1029/2008GL035201
- 498 Furth, H. P., Killeen, J., & Rosenbluth, M. N. (1963, April). Finite-Resistivity In-
499 stabilities of a Sheet Pinch. *Physics of Fluids*, 6(4), 459-484. doi: 10.1063/1
500 .1706761
- 501 Gary, S. P., & Karimabadi, H. (2006, November). Linear theory of electron
502 temperature anisotropy instabilities: Whistler, mirror, and Weibel. *Jour-
503 nal of Geophysical Research (Space Physics)*, 111(A11), A11224. doi:
504 10.1029/2006JA011764
- 505 Goldman, M. V., Newman, D. L., Lapenta, G., Andersson, L., Gosling, J. T.,
506 Eriksson, S., ... Ergun, R. (2014, April). Čerenkov Emission of Quasi-
507 parallel Whistlers by Fast Electron Phase-Space Holes during Magnetic
508 Reconnection. *Physical Review Letters*, 112(14), 145002. doi: 10.1103/
509 PhysRevLett.112.145002
- 510 Goldreich, P., & Sridhar, S. (1995, January). Toward a Theory of Interstellar Tur-
511 bulence. II. Strong Alfvénic Turbulence. *Astrophysical Journal*, 438, 763. doi:
512 10.1086/175121
- 513 Graham, D. B., Vaivads, A., Khotyaintsev, Y. V., & Andr, M. (2016). Whistler
514 emission in the separatrix regions of asymmetric magnetic reconnection. *Jour-
515 nal of Geophysical Research: Space Physics*, 121(3), 1934-1954. Retrieved
516 from [https://agupubs.onlinelibrary.wiley.com/doi/abs/10.1002/
517 2015JA021239](https://agupubs.onlinelibrary.wiley.com/doi/abs/10.1002/2015JA021239) doi: 10.1002/2015JA021239
- 518 Guo, F., Li, H., Daughton, W., & Liu, Y.-H. (2014, October). Formation of Hard
519 Power Laws in the Energetic Particle Spectra Resulting from Relativistic
520 Magnetic Reconnection. *Physical Review Letters*, 113(15), 155005. doi:
521 10.1103/PhysRevLett.113.155005
- 522 Gusakov, E. Z., & Surkov, A. V. (2007, May). Induced backscattering in an inhomog-
523 eneous plasma at the upper hybrid resonance. *Plasma Physics and Controlled
524 Fusion*, 49(5), 631-639. doi: 10.1088/0741-3335/49/5/005
- 525 Hesse, M., Kuznetsova, M., & Birn, J. (2001, December). Particle-in-cell simulations
526 of three-dimensional collisionless magnetic reconnection. *Journal of Geophysics
527 Research*, 106, 29831-29842. doi: 10.1029/2001JA000075
- 528 Holman, G. D., Aschwanden, M. J., Aurass, H., Battaglia, M., Grigis, P. C., Kontar,
529 E. P., ... Zharkova, V. V. (2011, September). Implications of X-ray Observa-
530 tions for Electron Acceleration and Propagation in Solar Flares. *Space Science
531 Reviews*, 159, 107-166. doi: 10.1007/s11214-010-9680-9
- 532 Howes, G. G., Dorland, W., Cowley, S. C., Hammett, G. W., Quataert, E.,
533 Schekochihin, A. A., & Tatsuno, T. (2008, February). Kinetic Simulations
534 of Magnetized Turbulence in Astrophysical Plasmas. *Physical Review Letters*,
535 100(6), 065004. doi: 10.1103/PhysRevLett.100.065004
- 536 Huang, C., Lu, Q., Wang, R., Guo, F., Wu, M., Lu, S., & Wang, S. (2017, feb). De-
537 velopment of turbulent magnetic reconnection in a magnetic island. *The As-
538 trophysical Journal*, 835(2), 245. Retrieved from [https://doi.org/10.3847/
539 2F1538-4357/2F835%2F2%2F245](https://doi.org/10.3847/2F1538-4357/2F835%2F2%2F245) doi: 10.3847/1538-4357/835/2/245
- 540 Huang, Y.-M., & Bhattacharjee, A. (2010). Scaling laws of resistive magne-
541 tohydrodynamic reconnection in the high-lundquist-number, plasmoid-
542 unstable regime. *Physics of Plasmas*, 17(6), 062104. Retrieved from
543 <https://doi.org/10.1063/1.3420208> doi: 10.1063/1.3420208
- 544 Hurford, G. J., Krucker, S., Lin, R. P., Schwartz, R. A., Share, G. H., & Smith,
545 D. M. (2006, June). Gamma-Ray Imaging of the 2003 October/November So-
546 lar Flares. *Astrophysical Journal, Letters*, 644, L93-L96. doi: 10.1086/505329
- 547 Hurford, G. J., Schwartz, R. A., Krucker, S., Lin, R. P., Smith, D. M., & Vilmer,
548 N. (2003, October). First Gamma-Ray Images of a Solar Flare. *Astrophysical*

- 549 *Journal, Letters*, 595, L77-L80. doi: 10.1086/378179
- 550 Jaroschek, C. H., Treumann, R. A., Lesch, H., & Scholer, M. (2004, March). Fast
551 reconnection in relativistic pair plasmas: Analysis of particle acceleration in
552 self-consistent full particle simulations. *Physics of Plasmas*, 11(3), 1151-1163.
553 doi: 10.1063/1.1644814
- 554 Karimabadi, H., Dorelli, J., Roytershteyn, V., Daughton, W., & Chacón, L. (2011,
555 July). Flux Pileup in Collisionless Magnetic Reconnection: Bursty Interaction
556 of Large Flux Ropes. *Physical Review Letters*, 107(2), 025002. doi: 10.1103/
557 PhysRevLett.107.025002
- 558 Karimabadi, H., Roytershteyn, V., Daughton, W., & Liu, Y.-H. (2013, October).
559 Recent Evolution in the Theory of Magnetic Reconnection and Its Con-
560 nnection with Turbulence. *Space Science Reviews*, 178(2-4), 307-323. doi:
561 10.1007/s11214-013-0021-7
- 562 Khabarova, O., Zank, G. P., Li, G., le Roux, J. A., Webb, G. M., Dosch, A., & Ma-
563 landraki, O. E. (2015, August). Small-scale Magnetic Islands in the Solar
564 Wind and Their Role in Particle Acceleration. I. Dynamics of Magnetic Islands
565 Near the Heliospheric Current Sheet. *Astrophysical Journal*, 808, 181. doi:
566 10.1088/0004-637X/808/2/181
- 567 Khabarova, O., Zharkova, V., Xia, Q., & Malandraki, O. E. (2020, may). Coun-
568 terstreaming strahls and heat flux dropouts as possible signatures of local
569 particle acceleration in the solar wind. *The Astrophysical Journal*, 894(1),
570 L12. Retrieved from <https://doi.org/10.3847/2F2041-8213/2Fab8cb8> doi:
571 10.3847/2041-8213/ab8cb8
- 572 Khabarova, O. V., Zank, G. P., Malandraki, O. E., Li, G., le Roux, J. A., & Webb,
573 G. M. (2017, January). Observational evidence for local particle acceleration
574 associated with magnetically confined magnetic islands in the heliosphere - a
575 review. *Sun and Geosphere*, 12, 23-30.
- 576 Khotyaintsev, Y. V., Vaivads, A., André, M., Fujimoto, M., Retinò, A., &
577 Owen, C. J. (2010, Oct). Observations of slow electron holes at a mag-
578 netic reconnection site. *Phys. Rev. Lett.*, 105, 165002. Retrieved from
579 <https://link.aps.org/doi/10.1103/PhysRevLett.105.165002> doi:
580 10.1103/PhysRevLett.105.165002
- 581 Lapenta, G. (2008, June). Self-Feeding Turbulent Magnetic Reconnection
582 on Macroscopic Scales. *Physical Review Letters*, 100(23), 235001. doi:
583 10.1103/PhysRevLett.100.235001
- 584 Lapenta, G., & Brackbill, J. U. (1997, December). A kinetic theory for the drift-kink
585 instability. *Journal of Geophysics Research*, 102(A12), 27099-27108. doi: 10
586 .1029/97JA02140
- 587 Lapenta, G., Markidis, S., Divin, A., Goldman, M. V., & Newman, D. L. (2011,
588 September). Bipolar electric field signatures of reconnection separatrices for a
589 hydrogen plasma at realistic guide fields. *Geophysics Research Letters*, 38(17),
590 L17104. doi: 10.1029/2011GL048572
- 591 Lapenta, G., Pucci, F., Goldman, M. V., & Newman, D. L. (2020, January). Lo-
592 cal Regimes of Turbulence in 3D Magnetic Reconnection. *Astrophysical Jour-
593 nal*, 888(2), 104. doi: 10.3847/1538-4357/ab5a86
- 594 Le, A., Egedal, J., Ohia, O., Daughton, W., Karimabadi, H., & Lukin, V. S. (2013,
595 Mar). Regimes of the electron diffusion region in magnetic reconnection.
596 *Phys. Rev. Lett.*, 110, 135004. Retrieved from [https://link.aps.org/doi/
597 10.1103/PhysRevLett.110.135004](https://link.aps.org/doi/10.1103/PhysRevLett.110.135004) doi: 10.1103/PhysRevLett.110.135004
- 598 Li, W. Y., Graham, D. B., Khotyaintsev, Y. V., Vaivads, A., André, M., Min, K.,
599 ... Burch, J. L. (2020, January). Electron Bernstein waves driven by electron
600 crescents near the electron diffusion region. *Nature Communications*, 11, 141.
601 doi: 10.1038/s41467-019-13920-w
- 602 Li, X., Guo, F., Li, H., Stanier, A., & Kilian, P. (2019, October). Formation of
603 Power-law Electron Energy Spectra in Three-dimensional Low- β Magnetic

- 604 Reconnection. *Astrophysical Journal*, 884(2), 118. doi: 10.3847/1538-4357/
605 ab4268
- 606 Lin, J., Ko, Y.-K., Sui, L., Raymond, J. C., Stenborg, G. A., Jiang, Y., ... Man-
607 cuso, S. (2005, April). Direct Observations of the Magnetic Reconnection Site
608 of an Eruption on 2003 November 18. *Astrophysical Journal*, 622, 1251-1264.
609 doi: 10.1086/428110
- 610 Lin, R. P., Krucker, S., Hurford, G. J., Smith, D. M., Hudson, H. S., Holman, G. D.,
611 ... Vilmer, N. (2003, October). RHESSI Observations of Particle Acceleration
612 and Energy Release in an Intense Solar Gamma-Ray Line Flare. *Astrophysical*
613 *Journal, Letters*, 595, L69-L76. doi: 10.1086/378932
- 614 Loureiro, N. F., Cowley, S. C., Dorland, W. D., Haines, M. G., & Schekochihin,
615 A. A. (2005, December). X-Point Collapse and Saturation in the Nonlinear
616 Tearing Mode Reconnection. *Physical Review Letters*, 95(23), 235003. doi:
617 10.1103/PhysRevLett.95.235003
- 618 Loureiro, Nuno F., & Boldyrev, Stanislav. (2017, June). Role of Magnetic Reconnec-
619 tion in Magnetohydrodynamic Turbulence. *Physical Review Letters*, 118(24),
620 245101. doi: 10.1103/PhysRevLett.118.245101
- 621 Markidis, S., Lapenta, G., Divin, A., Goldman, M., Newman, D., & Andersson,
622 L. (2012, March). Three dimensional density cavities in guide field colli-
623 sionless magnetic reconnection. *Physics of Plasmas*, 19(3), 032119. doi:
624 10.1063/1.3697976
- 625 Muñoz, P. A., & Büchner, J. (2016, October). Non-Maxwellian electron distri-
626 bution functions due to self-generated turbulence in collisionless guide-field
627 reconnection. *Physics of Plasmas*, 23(10), 102103. doi: 10.1063/1.4963773
- 628 Ng, J., Egedal, J., Le, A., & Daughton, W. (2012). Phase space structure of the
629 electron diffusion region in reconnection with weak guide fields. *Physics*
630 *of Plasmas*, 19(11), 112108. Retrieved from [https://doi.org/10.1063/
631 1.4766895](https://doi.org/10.1063/1.4766895) doi: 10.1063/1.4766895
- 632 Ng, J., Egedal, J., Le, A., Daughton, W., & Chen, L.-J. (2011, Feb). Kinetic struc-
633 ture of the electron diffusion region in antiparallel magnetic reconnection.
634 *Phys. Rev. Lett.*, 106, 065002. Retrieved from [https://link.aps.org/doi/
635 10.1103/PhysRevLett.106.065002](https://link.aps.org/doi/10.1103/PhysRevLett.106.065002) doi: 10.1103/PhysRevLett.106.065002
- 636 Nishizuka, N., Karlický, M., Janvier, M., & Bárta, M. (2015, February). Particle Ac-
637 celeration in Plasmoid Ejections Derived from Radio Drifting Pulsating Struc-
638 tures. *Astrophysical Journal*, 799, 126. doi: 10.1088/0004-637X/799/2/126
- 639 Øieroset, M., Lin, R. P., Phan, T. D., Larson, D. E., & Bale, S. D. (2002, Oct). Ev-
640 idence for electron acceleration up to ~ 300 keV in the magnetic reconnection
641 diffusion region of earth's magnetotail. *Phys. Rev. Lett.*, 89, 195001. Retrieved
642 from <https://link.aps.org/doi/10.1103/PhysRevLett.89.195001> doi: 10
643 .1103/PhysRevLett.89.195001
- 644 Øieroset, M., Phan, T. D., Fujimoto, M., Lin, R. P., & Lepping, R. P. (2001, July).
645 In situ detection of collisionless reconnection in the Earth's magnetotail. *Nat-
646 ure*, 412(6845), 414-417. doi: 10.1038/35086520
- 647 Oka, M., Phan, T.-D., Krucker, S., Fujimoto, M., & Shinohara, I. (2010, May). Elec-
648 tron Acceleration by Multi-Island Coalescence. *Astrophysical Journal*, 714,
649 915-926. doi: 10.1088/0004-637X/714/1/915
- 650 Papadopoulos, K., & Palmadesso, P. (1976). Excitation of lower hybrid waves
651 in a plasma by electron beams. *The Physics of Fluids*, 19(4), 605-606. Re-
652 trieved from <https://aip.scitation.org/doi/abs/10.1063/1.861501> doi:
653 10.1063/1.861501
- 654 Phan, T. D., Bale, S. D., Eastwood, J. P., Lavraud, B., Drake, J. F., Oieroset, M.,
655 ... Velli, M. (2020, February). Parker Solar Probe In Situ Observations of
656 Magnetic Reconnection Exhausts during Encounter 1. *Astrophysical Journal,
657 Supplement*, 246(2), 34. doi: 10.3847/1538-4365/ab55ee
- 658 Priest, E., & Forbes, T. (2000). *Magnetic Reconnection*. Cambridge University

- 659 Press, UK.
- 660 Pritchett, P. L., & Coroniti, F. V. (2004, January). Three-dimensional collisionless
661 magnetic reconnection in the presence of a guide field. *Journal of Geophysical*
662 *Research (Space Physics)*, *109*, A01220. doi: 10.1029/2003JA009999
- 663 Rogers, B. N., Drake, J. F., & Shay, M. A. (2000, October). The onset of turbulence
664 in collisionless magnetic reconnection. *Geophysics Research Letters*, *27*(19),
665 3157-3160. doi: 10.1029/2000GL000038
- 666 Scholer, M., Sidorenko, I., Jaroschek, C. H., Treumann, R. A., & Zeiler, A. (2003).
667 Onset of collisionless magnetic reconnection in thin current sheets: Three-
668 dimensional particle simulations. *Physics of Plasmas*, *10*(9), 3521-3527. Re-
669 trieved from <https://doi.org/10.1063/1.1597494> doi: 10.1063/1.1597494
- 670 Shay, M. A., Phan, T. D., Haggerty, C. C., Fujimoto, M., Drake, J. F., Malakit, K.,
671 ... Swisdak, M. (2016). Kinetic signatures of the region surrounding the x line
672 in asymmetric (magnetopause) reconnection. *Geophysical Research Letters*,
673 *43*(9), 4145-4154. Retrieved from [https://agupubs.onlinelibrary.wiley](https://agupubs.onlinelibrary.wiley.com/doi/abs/10.1002/2016GL069034)
674 [.com/doi/abs/10.1002/2016GL069034](https://agupubs.onlinelibrary.wiley.com/doi/abs/10.1002/2016GL069034) doi: 10.1002/2016GL069034
- 675 Silin, I., & Büchner, J. (2006, January). Three-dimensional Vlasov-code simulations
676 of magnetopause-like current sheets. *Advances in Space Research*, *37*(7), 1354-
677 1362. doi: 10.1016/j.asr.2005.05.025
- 678 Sironi, L., & Spitkovsky, A. (2014, Mar). Relativistic Reconnection: An Efficient
679 Source of Non-thermal Particles. *Astrophysical Journal, Letters*, *783*(1), L21.
680 doi: 10.1088/2041-8205/783/1/L21
- 681 Siversky, T. V., & Zharkova, V. V. (2009, October). Particle acceleration in a re-
682 connecting current sheet: PIC simulation. *Journal of Plasma Physics*, *75*, 619-
683 636. doi: 10.1017/S0022377809008009
- 684 Somov, B. V. (Ed.). (2000). *Cosmic Plasma Physics* (Vol. 251). doi: 10.1007/978-94
685 -015-9592-6
- 686 Song, H.-Q., Chen, Y., Li, G., Kong, X.-L., & Feng, S.-W. (2012, April). Co-
687 alescence of Macroscopic Magnetic Islands and Electron Acceleration
688 from STEREO Observation. *Physical Review X*, *2*(2), 021015. doi:
689 10.1103/PhysRevX.2.021015
- 690 Takasao, S., Asai, A., Isobe, H., & Shibata, K. (2012, January). Simultane-
691 ous Observation of Reconnection Inflow and Outflow Associated with the
692 2010 August 18 Solar Flare. *Astrophysical Journal, Letters*, *745*, L6. doi:
693 10.1088/2041-8205/745/1/L6
- 694 Verboncoeur, J. P., Langdon, A. B., & Gladd, N. T. (1995, May). An object-
695 oriented electromagnetic PIC code. *Computer Physics Communications*, *87*,
696 199-211. doi: 10.1016/0010-4655(94)00173-Y
- 697 Vilmer, N., MacKinnon, A. L., & Hurford, G. J. (2011, September). Properties of
698 Energetic Ions in the Solar Atmosphere from γ -Ray and Neutron Observations.
699 *Space Science Reviews*, *159*, 167-224. doi: 10.1007/s11214-010-9728-x
- 700 Wang, R., Lu, Q., Nakamura, R., Huang, C., Du, A., Guo, F., ... Wang, S. (2016,
701 3 1). Coalescence of magnetic flux ropes in the ion diffusion region of magnetic
702 reconnection. *Nature Physics*, *12*(3), 263-267. doi: 10.1038/nphys3578
- 703 Wang, S., Chen, L.-J., Bessho, N., Kistler, L. M., Shuster, J. R., & Guo, R. (2016).
704 Electron heating in the exhaust of magnetic reconnection with negligible guide
705 field. *Journal of Geophysical Research: Space Physics*, *121*(3), 2104-2130.
706 Retrieved from [https://agupubs.onlinelibrary.wiley.com/doi/abs/](https://agupubs.onlinelibrary.wiley.com/doi/abs/10.1002/2015JA021892)
707 [10.1002/2015JA021892](https://agupubs.onlinelibrary.wiley.com/doi/abs/10.1002/2015JA021892) doi: 10.1002/2015JA021892
- 708 Xia, Q., & Zharkova, V. (2020, March). Particle acceleration in coalescent and
709 squashed magnetic islands II. Particle-in-cell approach. *Astronomy and Astro-*
710 *physics*, *635*, A116.
- 711 Zank, G. P., le Roux, J. A., Webb, G. M., Dosch, A., & Khabarova, O. (2014, De-
712 cember). Particle Acceleration via Reconnection Processes in the Supersonic
713 Solar Wind. *Astrophysical Journal*, *797*, 28. doi: 10.1088/0004-637X/797/1/

714
715
716
717
718
719
720
721
722
723
724
725
726
727
728
729
730
731
732
733
734
735
736
737
738
739
740
741
742
743
744
745
746
747
748
749
750
751
752
753
754
755
756
757

- Zenitani, S., & Hoshino, M. (2008, April). The Role of the Guide Field in Relativistic Pair Plasma Reconnection. *Astrophysical Journal*, *677*(1), 530-544. doi: 10.1086/528708
- Zhang, Q., Drake, J. F., & Swisdak, M. (2019). Instabilities and turbulence in low-guide field reconnection exhausts with kinetic riemann simulations. *Physics of Plasmas*, *26*(10), 102115. Retrieved from <https://doi.org/10.1063/1.5121782> doi: 10.1063/1.5121782
- Zharkova, V., & Khabarova, O. (2015, April). Additional acceleration of solar-wind particles in current sheets of the heliosphere. *Annales Geophysicae*, *33*, 457-470. doi: 10.5194/angeo-33-457-2015
- Zharkova, V. V., & Agapitov, O. V. (2009, April). The effect of magnetic topology on particle acceleration in a three-dimensional reconnecting current sheet: a test-particle approach. *Journal of Plasma Physics*, *75*, 159-181. doi: 10.1017/S002237780800771X
- Zharkova, V. V., Arzner, K., Benz, A. O., Browning, P., Dauphin, C., Emslie, A. G., ... Vlahos, L. (2011, September). Recent Advances in Understanding Particle Acceleration Processes in Solar Flares. *Space Science Reviews*, *159*, 357-420. doi: 10.1007/s11214-011-9803-y
- Zharkova, V. V., & Gordovskyy, M. (2004, April). Particle Acceleration Asymmetry in a Reconnecting Nonneutral Current Sheet. *Astrophysical Journal*, *604*, 884-891. doi: 10.1086/381966
- Zharkova, V. V., & Gordovskyy, M. (2005, January). Energy spectra of particles accelerated in a reconnecting current sheet with the guiding magnetic field. *Monthly Notices of the RAS*, *356*, 1107-1116. doi: 10.1111/j.1365-2966.2004.08532.x
- Zharkova, V. V., & Khabarova, O. V. (2012, June). Particle Dynamics in the Reconnecting Heliospheric Current Sheet: Solar Wind Data versus Three-dimensional Particle-in-cell Simulations. *Astrophysical Journal*, *752*, 35. doi: 10.1088/0004-637X/752/1/35
- Zhong, J. Y., Lin, J., Li, Y. T., Wang, X., Li, Y., Zhang, K., ... Zhang, J. (2016). Relativistic electrons produced by reconnecting electric fields in a laser-driven bench-top solar flare. *The Astrophysical Journal Supplement Series*, *225*(2), 30. Retrieved from <http://stacks.iop.org/0067-0049/225/i=2/a=30>
- Zhou, M., Li, H., Deng, X., Huang, S., Pang, Y., Yuan, Z., ... Tang, R. (2014). Characteristic distribution and possible roles of waves around the lower hybrid frequency in the magnetotail reconnection region. *Journal of Geophysical Research: Space Physics*, *119*(10), 8228-8242. Retrieved from <https://agupubs.onlinelibrary.wiley.com/doi/abs/10.1002/2014JA019978> doi: 10.1002/2014JA019978
- Zong, Q.-G., Fritz, T. A., Pu, Z. Y., Fu, S. Y., Baker, D. N., Zhang, H., ... Reme, H. (2004, September). Cluster observations of earthward flowing plasmoid in the tail. *Geophysics Research Letters*, *31*, L18803. doi: 10.1029/2004GL020692